NIH Public Access
Author Manuscript
Biomaterials. Author manuscript; available in PMC 2012 February 1.

Published in final edited form as:
Biomaterials. 2011 February ; 32(6): 1731–1737. doi:10.1016/j.biomaterials.2010.10.059.

Effects of particle size on toll-like receptor 9-mediated cytokine profiles

Helen C. Chen, **Bingbing Sun**, **Kenny K. Tran**, and **Hong Shen***
Department of Chemical Engineering, University of Washington, 353 Benson Hall, Box 351750, Seattle, WA 98195, USA

Abstract

Biomaterials interface with toll-like receptor (TLR) 9-mediated innate immunity in a wide range of medical applications, such as tissue implants and drug delivery systems. The stimulation of TLR9 can lead to two different signaling pathways, resulting in the generation of proinflammatory cytokines (i.e. IL-6) and/or type I interferons (IFNs, i.e. IFN-α). These two categories of cytokines differentially influence both innate and adaptive immunity. Although particle size is known to be a critical parameter of biomaterials, its role in TLR9-mediated cytokine profiles is not clear. Here, we examined how the size of biomaterials impacted cytokine profiles by using polystyrene particles of defined sizes as model carriers for TLR9 agonists (CpG oligonucleotides (CpG ODNs)). CpG ODNs bound to nano- to submicro- particles stimulated the production of both IL-6 and IFN-α, while those bound to microparticles resulted in IL-6 secretions only. The differential TLR9-mediated cytokine profiles were attributed to the pH of endosomes that particles trafficked to. The magnitude of IFN-α production was highly sensitive to the change in endosomal pH in comparison to that of IL-6. Our results define two critical design variables, size and the ability to modulate endosomal pH, for the engineering of biomaterials that potentially interface with TLR9-mediated innate immunity. The fine control of these two variables will allow us to fully exploit the beneficial facets of TLR9-mediated innate immunity while minimizing undesirable side effects.

Keywords

non-viral DNA delivery; toll-like receptor; vaccine; immunotherapy; tissue engineering

1. Introduction

Toll-like receptors (TLRs) have been well recognized for their pivotal role in the detection of pathogen associated molecular patterns (PAMPs). Twelve TLRs, each detecting a distinct set of PAMPs, have been identified in mammals [1]. TLR9 was first identified as a sensor for bacterial DNA [2], which contains unmethylated CpG motifs. Subsequently, a broad range of natural TLR9 ligands has been identified, including DNA derived from dead cells [3,4], fungi [5,6], viruses [7–9], and chromatin-IgG complexes [10,11]. A recent study has suggested that TLR9 can detect any single stranded DNA [12]. Since its initial discovery, TLR9 has become one of the central targets for mediating immune responses. Many different types of synthetic TLR9 ligands, CpG motif-containing oligonuleotides (CpG

*Corresponding author. Tel.: +1 206 543 5961. hs24@u.washington.edu (H. Shen).

Publisher's Disclaimer: This is a PDF file of an unedited manuscript that has been accepted for publication. As a service to our customers we are providing this early version of the manuscript. The manuscript will undergo copyediting, typesetting, and review of the resulting proof before it is published in its final citable form. Please note that during the production process errors may be discovered which could affect the content, and all legal disclaimers that apply to the journal pertain.

NIH-PA Author Manuscript
NIH-PA Author Manuscript
NIH-PA Author Manuscript

NIH-PA Author Manuscript

NIH-PA Author Manuscript

NIH-PA Author Manuscript

ODNs), have been characterized and utilized as adjuvants for vaccines [13–16] and microbicides [17–20] against pathogen infections.

The role of TLR9 in the design of biomaterials for medical applications is implicated in three main areas: (1) particulate systems that deliver TLR9 ligands for vaccination or microbicidal activities [21–26]; (2) non-viral DNA delivery systems, which can control the interaction of DNA with TLR9 and thus minimize their immunogenicity for their application in gene therapy [27–31]; (3) tissue implants, which release degraded or eroded biomaterial fragments. These fragments are potentially deposited with DNA derived from bacteria or dead cells and endocytosed by phagocytic cells (such as macrophages). As a result, the endocytosed DNA can trigger the TLR9-based innate immune system and lead to the failure of tissue implants [32–34].

TLR9 is situated in the endoplasmic reticulum (ER) and recruited to endosomal/lysosomal compartments upon the endocytosis of pathogens or particulates [35]. The stimulation of TLR9 can lead to two distinct signaling pathways in which two transcription factors, NF-κB and IRF-7, are translocated into the nucleus, resulting in the generation of proinflammatory cytokines (such as IL-6 and IL-12) and/or type I interferons (IFNs) (such as IFN-α), respectively [1]. These two types of cytokines play independent roles in the induction and maintenance of innate and adaptive immune responses. For example, IL-6 is a key mediator of the acute phase response [36]. IL-6 is critical in the proliferation, differentiation and survival of B cells, $CD4^+$ T cell differentiation to Th2 cells [37]. Type I IFNs, such as IFN-α, inhibit viral replication and induce apoptosis to clear infected cells. IFN-α promotes the proliferation and function of $CD8^+$ T cells, maintains $CD4^+$ Th1/Th2 cell populations. IFN-α plays a key role in the pathogenesis of the autoimmune disease, systemic lupus erythematosus (SLE) as well [38]. Additionally, proinflammatory cytokines and type I IFNs play differential roles in bone tissue engineering. IL-6 promotes osteoclast formation [39], whereas type I IFNs, such as IFN-α and IFN-β, inhibit osteoclast differentiation [40]. Due to the functional diversity of proinflammatory cytokines and type I IFNs, the ability to control the TLR9-mediated signaling pathways is essential for the design of biomaterials that interface with TLR9-based innate immunity.

The size of biomaterials is considered to be critical for the three aforementioned medical applications because it affects the level of retention in tissues [41,42] and the efficiency of cellular uptake [43–45]. Others and we have demonstrated that the size of biomaterials also affects their intracellular trafficking [46–48]. Given the critical role of the intracellular location of TLR9 ligands which dictates the subsequent induction of signaling pathways [49–51], we hypothesized that the size of biomaterials could affect the TLR9-mediated cytokine profiles. The cytokine profiles in turn would impact the immunogenicity of biomaterials and lead to either beneficial or detrimental effects depending on the clinical applications of the designed biomaterials.

To test this hypothesis, in this study, we used polystyrene particles of defined sizes as model carriers for CpG ODNs to investigate the effect of particle size on the cytokine profiles mediated through the TLR9 signaling pathway and possible mechanisms involved.

2. Materials and Methods

2.1 Cell culture

A dendritic cell line, BC-1 (a gift from Dr. Yoshiki Yanagawa), was maintained in Isocove's Modified Dulbecco's Medium (IMDM) supplemented with 20% NIH-3T3 supernatant, 4 mM L-glutamine, 50 μM 2-mercaptoethanol, 5% granulocyte-macrophage colony-stimulating factor (GM-CSF)–containing supernatants, 100 units/ml penicillin and 100 μg/

NIH-PA Author Manuscript

NIH-PA Author Manuscript

NIH-PA Author Manuscript

ml streptomycin. The fibroblast cell line, NIH-3T3, was maintained in IMDM supplemented with 10% fetal bovine serum (FBS), 100 units/ml penicillin and 100 μg/ml streptomycin. Cells were maintained at 37 °C under an atmosphere with 5% CO_2. 5% GM-CSF-containing supernatants were obtained from GM-CSF conditioned medium from the GM-CSF-secreting mouse cell line J558L.

2.2 Preparation and characterization of ODN-coated PS particles (ODN-PLL-PS)

Fluorescent polystyrene (PS) particles (Polysciences, Inc., Warrington, PA) of different sizes, 100 nm, 500 nm, and 3 μm in diameter, were used as model CpG ODN carriers. The particles were first coated with poly-L-lysine (PLL; Sigma-Aldrich, Inc., Saint Louis, MO; MW = 30,000–70,000 g/mol), a cationic polymer, to facilitate the adsorption of ODNs onto particles. PLL-coated particles are designated as PLL-PS. For 100 nm particles, 250 μl of PS (2.8×10^{12} particles per ml in 10 mM NaCl) was added drop-wise to an equal volume of PLL (0.8 mg/ml in 10 mM NaCl) under constant vortexing. For 500 nm and 3 μm particles, 1 ml of PS (2×10^{10} 500 nm particles per ml, 5×10^{8} 3 μm particles per ml) was added drop-wise to 1 ml of PLL (0.15 mg/ml (500 nm), 0.25 mg/ml (3 μm)). The final reaction volume was 500 μl for 100 nm particles, and 2 ml for 500 nm and 3 μm particles. The adsorption was conducted for 1 h at room temperature (RT) and the reaction vessel was vortexed every 15 min. PLL-PS was washed three times in 10 mM NaCl by centrifugation at 4 °C, 8000 rcf for 2 h, 300 rcf for 1 h, and 25 rcf for 30 min for 100 nm, 500 nm, and 3 μm particles, respectively. 60% of 100 and 500 nm particles were recovered, and 100% of 3 μm particles were recovered. The duration and centrifuge speed were optimized to obtain mono-dispersed particles. CpG ODNs 1826 and 2216 (TriLink BioTechnologies, San Diego, CA) were attached onto PLL-PS by using the same procedures and reaction volumes as used for the coating of PLL onto particles. The final reaction mixtures contained 4×10^{11} particles per ml and 86 μg/ml ODN-1826, 4.5×10^{9} particles per ml and 40 μg/ml ODN-1826, and 1×10^{8} particles per ml and 33 μg/ml ODN-1826 for 100 nm, 500 nm, and 3 μm particles, respectively. The attachment of ODN 2216 onto PLL-PS was similar to that of ODN 1826. ODN-coated particles (ODN-PLL-PS are denoted as 1826-PLL-PS or 2216-PLL-PS, depending on the type of CpG ODN) were washed in the same manner as stated above. All of the washes were collected for further analysis of non-bound ODNs. The sequences of ODNs 1826 and 2216 were: 5′tcc atg acg ttc ctg acg tT3′ and 5′ggG GGA CGA TCG TCg ggg gG3′, respectively. Lowercase letters denote a phosphorothioate backone, and uppercase letters denote a phosphodiester backbone.

A Zetasizer Nano ZS (Malvern Instruments, Westborough, MA) was used to characterize the size distribution and zeta potential of the particles. 100 nm, 500 nm, and 3 μm particles were prepared at 3×10^{10}, 5×10^{7}, and 4×10^{6} particles per ml, respectively, in 10 mM NaCl with a pH of 5.9. Scanning electron microscopy (SEM) was used to confirm the particle size. SEM samples of particles were prepared in Milli-Q water, dried, sputter-coated with 12 nm of platinum using a SPI Sputter Coater (Structure Probe, Inc., West Chester, PA), and analyzed using a JEOL 7000 SEM with a beam voltage of 10.0 kV (Electron Microscopy Center, University of Washington).

2.3 Quantification of the surface density of ODNs on ODN-PLL-PS particles

The surface density of ODNs was determined by quantifying both the total amount of ODNs adsorbed and the number of fluorescent particles. The OliGreen Assay Kit for ssDNA (Invitrogen, Frederick, MD) was used to measure non-bound ODNs in the adsorption reaction solutions and washes for the indirect determination of the amount of ODNs adsorbed onto particles. The number of 100 and 500 nm particles was quantified by fluorescence spectrometry. For 100 nm particles, the particles were suspended in 10 mM NaCl and the fluorescent intensity of the particle suspension was directly measured. For 500

NIH-PA Author Manuscript

NIH-PA Author Manuscript

NIH-PA Author Manuscript

nm particles, particles were dried under a stream of air, dried for an additional 4 h at RT, and then dissolved in chloroform overnight. The fluorescent intensity of dissolved particles in chloroform was subsequently determined. For both sizes of particles, a series of standards with a known number of particles were used to construct standard curves. 3 μm particles were directly counted by a hemocytometer.

2.4 Regulation and measurement of endosomal pH

The pH of endosomes was controlled by exposing DCs to medium containing a weak acid, NH_4Cl [52]. The endosomal pH was measured by using a fluorescence ratiometric method that has been previously established [46]. Briefly, 100 nm amine-functionalized polystyrene particles (Polysciences, Inc., Warrington, PA) were reacted with pH-sensitive fluorescein isothiocyanate (FITC; Sigma-Aldrich, Inc., Saint Louis, MO), and pH-insensitive Alexa Fluor 647 carboxylic acid, succinimidyl ester (Invitrogen, Frederick, MD) for 4 h at RT in 0.1 M sodium carbonate buffer (pH = 8.3). The conjugation reaction was quenched with the addition of NH_4Cl, and particles were washed three times in phosphate buffered saline (PBS, pH = 7.4). To ensure the equivalent uptake of particles, DCs were seeded in a 6-well plate at a density of 3×10^6 cells per well. DCs were pulsed with particles for 6 h. Afterwards, cells were harvested and aliquoted at 2×10^5 cells per aliquot. One set of aliquots was incubated in different concentrations of NH_4Cl in IMDM supplemented with 0.5% FBS for 1 h at 37 °C. The other set, used for constructing a standard curve, was fixed with 4% paraformaldehyde (PFA) for 20 min at RT, permeabilized with 0.1% Triton X-100 for 2 min at RT, and incubated in 0.1 M citrate buffer solutions of known pH values for 1 h at RT. Citrate buffer solutions were prepared in Dulbecco's phosphate buffered saline (DPBS). Cell suspensions were analyzed using a FACsCanto (Cell Analysis Facility, University of Washington). The geometric mean fluorescent intensity (gMFI) of cells was determined by FlowJo (Treestar, Inc., Ashland, OR). The ratio of gMFI of FITC to that of Alexa Fluor 647 was compared to the standard curve constructed in the citrate buffers with known pH values to obtain the endosomal pH of each sample.

2.5 Stimulation of DCs with ODN-PLL-PS

DCs were seeded at a density of 2.5×10^5 cells per well in a 24-well plate. Soluble ODNs (0.005 mg/ml), 1826- and 2216-PLL-PS (100 nm, 500 nm, 3 μm) were added to cells in 500 μl medium in the absence or presence of designated concentrations of NH_4Cl. After 24 h of incubation at 37 °C, cell supernatants were collected and stored at −20 °C until further analysis.

2.6 Measurement of cytokine concentrations

Cell supernatants were analyzed by enzyme-linked immunosorbent assay (ELISA) for the quantification of IL-6 and IFN-α. The procedures for the ELISA for IL-6 were adapted from the manufacturer's protocol (eBiosciences, San Diego, CA). The procedures for IFN-α were described previously [8,53].

2.7 Statistical analysis

All experiments were repeated two to three times. The two-tailed and unpaired Student's *t* test was used to analyze the differences between experimental groups as specified. A value of $p < 0.05$ was considered to be statistically significant.

NIH-PA Author Manuscript

NIH-PA Author Manuscript

NIH-PA Author Manuscript

3. Results

3.1 Characterization of ODN-PLL-PS particles

To examine the effect of particle size on the TLR9-mediated cytokine production, it was critical that ODN-PLL-PS maintained mono-dispersity and a defined size. Commercially available PS particles of defined sizes (Polydispersity Index (PDI) = 0.037 ± 0.032, 0.242 ± 0.010, 0.234 ± 0.038, for 100 nm, 500 nm, and 3 μm particles, respectively) were chosen as model ODN carriers. Because PS particles bear a negative surface charge, a cationic polymer was first adsorbed onto the surface of the particles to enhance the electrostatic adsorption of ODN onto particles. Several cationic polymers, such as poly(ethylenimine), chitosan, poly(2-dimethyl-amino)ethyl methacrylate (pDMAEMA), or poly-L-lysine (PLL), have been used to facilitate the attachment of DNA onto the carrier [54,55]. PLL was used in this study because PLL induced minimal escape of particles from endosomal compartments and did not affect the endosomal pH [56]. PLL concentrations were optimized in order to achieve mono-dispersed particles with the maximal coverage of PLL (Supplemental Figure 1). The PLL coating shifted the surface charge of the particles from a negative to a positive zeta potential. At the maximal coverage of PLL, the zeta potential was 45, 65, and 43 mV for 100 nm, 500 nm, and 3μm particles, respectively.

Mono-dispersed PLL-PS was subsequently complexed with ODNs to yield ODN-PLL-PS. The negatively charged phosphate groups of the ODN backbone were expected to interact with the amine group side chain of lysine and result in ODN adsorption onto PS particles [57]. The size and zeta potential of 100 nm 1826-PLL-PS at different solution concentrations of CpG ODNs are shown in Figure 1. At the lowest ODN concentration examined, 0.005 mg/ml, particles tended to aggregate; the measured particle diameter and surface charge was approximately 300 nm and −10.6 mV. At the highest ODN concentration examined, 0.05 mg/ml, electrostatic stability was achieved and aggregation was minimal; the measured diameter and zeta potential was 129 nm and −19.2 mV. 500 nm and 3 μm 1826-PLL-PS exhibited a similar trend. At the optimized ODN concentrations, as stated in the Materials and Methods section, 500 nm and 3 μm ODN-PLL-PS had a surface charge of approximately −32 and −39 mV, respectively, and measured diameters of 433 nm and 3.5 μm. The measured diameter of 500 nm ODN-PLL-PS was less than 500 nm by DLS, and 500 nm PLL-PS was approximately 500 nm. Therefore, the polyelectrolyte coating may have affected the size measurement by DLS. The type of CpG ODN (1826 or 2216) did not have a significant effect on the size and zeta potential of ODN-PLL-PS (data not shown). Optimized conditions were used to prepare mono-disperse particles of uniform sizes for all experiments.

3.2 Differential cytokine profiles induced by CpG ODNs

Two different classes of CpG ODNs, B (i.e. CpG ODN 1826) and A (i.e. CpG ODN 2216) were adsorbed onto particles of different sizes. While both ODN types induce cytokines through the stimulation of TLR9, type B is particularly effective at inducing proinflammatory cytokines, such as IL-6, but not type I IFNs [50,58], and type A is known to induce both proinflammatory cytokines and type I IFNs, such as IFN-α [50,59]. For CpG ODN 1826, regardless of the size of particles, only IL-6 but not IFN-α was induced (Supplemental Figure 2), which was consistent with what was observed with soluble CpG ODN 1826.

For CpG ODN 2216, both IL-6 and IFN-α were detected when ODNs were bound to 100 and 500 nm particles, which was again consistent with what was observed with soluble ODNs (Figure 2D, E, G, H). Surprisingly, when CpG ODN 2216 was bound to 3 μm particles, IFN-α was completely diminished within the wide range of the concentrations of

NIH-PA Author Manuscript

NIH-PA Author Manuscript

NIH-PA Author Manuscript

ODNs tested (Figure 2I), while IL-6 secretions remained at a significantly high level (Figure 2F). We note that we did not attempt to compare the efficiencies of stimulation of TLR9 by the three different sizes of particles because it is challenging to deliver equivalent amounts of ODNs due to the large difference in the surface area among the three particle sizes. Regardless of this issue, we have clearly demonstrated that ODNs bound to sub-micro and micro particles yield distinct cytokine profiles.

3.3 The effect of endosomal pH on cytokine profiles induced by CpG ODNs

Previous studies have suggested that pH plays a critical role in TLR9-mediated signaling. Both the recruitment of TLR9 into endosomal compartments and the interactions between TLR9 and its ligands require the acidification of the endosomes [35,60]. Cells treated with inhibitors of acidification of endosomes, such as chloroquine or bafilomycin, exhibit impaired TLR9 stimulation [8,60,61]. We have demonstrated that the initial pH of endosomal compartments where 3 μm particles reside is 6.0. After 30 min, it increased to 7 and remained at 7. In contrast, submicron particles reside in endosomal compartments of pH 5.0 to 6.0 [46]. We hypothesized that the pH of endosomal compartments might affect the cytokine profiles induced by CpG ODN 2216. We tested this hypothesis by exposing both soluble CpG ODN 2216 and 100 nm 2216-PLL-PS to a broad range of endosomal pH environments.

The addition of NH_4Cl to the cell culture medium can inhibit endosomal acidification due to the rapid transport of NH_3 across the endosomal membranes and the low permeability of NH_4^+ [52,62]. We first confirmed the change in pH of endosomal compartments while cells were exposed to different concentrations of NH_4Cl. As shown in Figure 3, the pH of endosomal compartments increased by 1.2 while the NH_4Cl concentration increased from 0 to 16 mM. The change in endosomal pH of DCs was consistent with a previous report on the change in endosomal pH of mouse peritoneal macrophages, although only 0.16 mM NH_4Cl was needed to increase the pH by 1.6 in macrophages [62]. This discrepancy may be because the regulation of pH by NH_4Cl is cell-type dependent. By varying the concentration of NH_4Cl, we were able to obtain a distribution of pH environments that spanned from 5.21 to 6.38 in DCs.

We then studied the effect of the endosomal pH environment on the production of cytokines. A gradual increase in endosomal pH (Figure 3) corresponded to a gradual decline in IFN-α production by both soluble ODN 2216 and 2216-PLL-PS (Figure 4A). For 2216-PLL-PS, the production of IFN-α reduced by 80% when the pH increased from 5.21 to 5.82. The production of IL-6, however, remained constant (Figure 4B). At pH = 6.38, the levels of both IL-6 and IFN-α were diminished. Subsequently, we tested whether the cellular uptake of 2216-PLL-PS was affected by the presence of NH_4Cl. The addition of NH_4Cl slightly reduced the cellular uptake at concentrations up to 16 mM, which resulted the endosomal pH of 6.38. However, there was not a significant difference in the level of cellular uptake at lower NH_4Cl concentrations, except at 16 mM (Supplemental Figure 3). At pH = 6.38, the cellular uptake of 2216-PLL-PS decreased (Supplemental Figure 3), which could contribute to the reduction in the level of both IL-6 and IFN-α. In addition, the recruitment of TLR9 to endosomes at pH = 6.38 may be impaired as suggested previously [35]. Our results demonstrate that the endosomal pH affected the TLR9-mediated cytokine profiles. Therefore, the distinct cytokine profiles exhibited by micro- and submicro- particles can be attributed to the endosomal pH they are exposed to.

4. Discussion

By using model submicro- and micro- PS particles as TLR9-ligand (CpG ODN) carriers, we investigated the effect of the size of biomaterials on the TLR9-mediated production of

NIH-PA Author Manuscript

NIH-PA Author Manuscript

NIH-PA Author Manuscript

cytokines. CpG ODN 2216 bound to 100 and 500 nm particles induced the production of both IL-6 and IFN-α. Surprisingly, when CpG ODN 2216 was bound to 3 μm particles, IFN-α secretions were not detected, though IL-6 secretions remained at a significantly high level. By correlating the cytokine production with the pH environment that particles of different sizes were exposed to, we further demonstrated that the endosomal pH regulated the cytokine profiles mediated through TLR9 stimulation. Our findings indicate that the size of biomaterials and the ability to regulate endosomal pH have a profound effect on the TLR9-mediated differential production of cytokines that regulate innate and adaptive immunity.

The intracellular location of TLR9 ligands has recently been shown to affect cytokine profiles. Honda et al. suggested that the retention of TLR9 agonists (CpG oligonucleotides) in early endosomal compartments led to a much higher level of type I IFNs than in late endosomal/lysosomal compartments [50]. Okuya et al. further confirmed this study and showed that the targeting of CpG ODNs to static early endosomes, which are a subpopulation of early endosomes and exhibit slow maturation kinetics and low mobility along microtubules [63], enhanced the generation of type I IFNs, but diminished the generation of proinflammatory cytokines [49]. Our previous study has shown that micrometer particles do not co-localize with LysoTracker, which was used to distinguish late endosomes and lysosomes from early endosomes, while submicrometer particles do [46]. We also confirmed that 3 μm particles were localized in early endosomes by using an early endosome-specific marker, early endosomal antigen-1 (EEA-1) (Supplemental Figure 4). The FITC-labeled 3 μm particles associated with EEA-1 (Supplemental Figure 4A). In addition, a cross-sectional image showing EEA-1 only (Supplemental Figure 4B) revealed ring-like structures that surrounded the particles, suggesting that the particles were contained within early endosomes.

Our results appeared to be inconsistent with the studies by Honda et al. [50] and Okuya et al. [49]. The inconsistent observations may arise from differences in carrier-specific intracellular trafficking and ODN release mechanisms. In this study, ODN-decorated PS particles of defined sizes were used. Our previous study showed that particles of different sizes were transported to different intracellular compartments that exhibited distinct kinetics of pH change and steady state pH. The correlation of cytokine production with the endosomal pH environment that TLR9 ligands were exposed to suggested that the endosomal pH affected TLR9-mediated cytokine profiles. In the study by Honda et al., the cationic liposome, N-[1-(2,3-Dioleoyloxy)propyl]-N,N,N-trimethylammonium methylsuflate (DOTAP), had been used as a CpG ODN carrier. It has been documented that the lipid membrane charge density and size of lipid-based DNA delivery systems determines the intracellular fate of lipoplexes [47,64,65]. In addition, the release of ODNs from DOTAP/ODN complexes is dependent on size and charge ratio, and is mediated by the fusogenic interaction between DOTAP and the anionic lipid membrane of intracellular compartments [66]. No detailed information in the study by Honda et al. was available to determine the size, charge ratio, and membrane charge density of the DOTAP/ODN complexes. In the study by Okuya et al., the heat-shock protein Hsp90 was used as the ODN carrier. However, the intracellular transport of heat-shock proteins remains elusive: endocytosed Hsps may transit through endosomes, into the cytoplasm, and/or into other intracellular vesicles [67,68], which can potentially affect TLR9-mediated signaling. It is clear that endosomal markers, such as EEA-1 and LysoTracker, are not sufficient to distinguish the intracellular compartments that the three TLR9-ligand carriers, i.e. PS, DOTAP, and Hsp90, are transported to. More detailed studies are required to determine whether the carriers used in all three studies reside in the same intracellular compartment. A recent model of the bifurcation of TLR9 signaling proposed by Sasai et al. suggested that the adaptor protein 3 (AP-3), which finely controlled the trafficking of TLR9 within the endosomal system, was essential for the activation of type I IFN genes [51]. An

NIH-PA Author Manuscript

NIH-PA Author Manuscript

NIH-PA Author Manuscript

understanding of how the carrier type and the dynamics of endosomal pH affect the recruitment of AP-3 to TLR9-residing compartments may reconcile the differences observed.

Previous studies have suggested that pH plays a critical role in TLR9-mediated signaling. Our results suggest an additional role of pH, that is, the endosomal pH affects the profiles of cytokines mediated by TLR9 activation. Carriers which possess the ability to modulate endosomal pH could potentially be used to regulate TLR9-mediated innate immunity. Collectively, our findings indicate that cytokine profiles may be manipulated by controlling the size and/or the composition of biomaterials.

5. Conclusion

In this study, we demonstrated that the size of particles affected the cytokine profiles mediated by TLR9 signaling pathways. By examining the pH of endosomes at which particles of different sizes trafficked to, we showed that type I IFNs, such as IFN-α, were much more sensitive to the change in endosomal pH compared to proinflammatory cytokines, such as IL-6. The role of TLR9 in the applications of biomaterials in medicine lies in delivery systems for vaccines, microbicides, and plasmid DNA and tissue implants. Our findings provide significant implications for two major design parameters: size and composition of biomaterials. The fine control of either or both parameters allows the exploitation of the beneficial aspects of TLR9-mediated innate immunity while minimizing unwanted side effects.

Supplementary Material

Refer to Web version on PubMed Central for supplementary material.

Acknowledgments

The authors gratefully acknowledge Dr. Shaoyi Jiang for the use of his DLS instrument, Hai Nguyen for helpful discussions on the optimization of ODN-coated particles, and Greg Martin (Keck Imaging Center, University of Washington) for assistance with image analysis. This study was funded by AI088597 from the National Institute of Allergy and Infectious Diseases (NIAID) and the Office of Research on Women's Health (ORWH), the NSF Career Award to H.S., and the NSF Graduate Research Fellowship to H. C. Chen. The content is solely the responsibility of the authors and does not necessarily represent the official views of NIAID, ORWH or NIH.

References

1. Akira S, Uematsu S, Takeuchi O. Pathogen recognition and innate immunity. Cell 2006;124:783–801. [PubMed: 16497588]
2. Hemmi H, Takeuchi O, Kawai T, Kaisho T, Sato S, Sanjo H, et al. A toll-like receptor recognizes bacterial DNA. Nature 2000;408:740–5. [PubMed: 11130078]
3. Means TK, Latz E, Hayashi F, Murali MR, Golenbock DT, Luster AD. Human lupus autoantibody-DNA complexes activate DCs through cooperation of CD32 and TLR9. J Clin Invest 2005;115:407–17. [PubMed: 15668740]
4. Barrat FJ, Meeker T, Gregorio J, Chan JH, Uematsu S, Akira S, et al. Nucleic acids of mammalian origin can act as endogenous ligands for toll-like receptors and may promote systemic lupus erythematosus. J Exp Med 2005;202:1131–9. [PubMed: 16230478]
5. Ramirez-Ortiz ZG, Specht CA, Wang JP, Lee CK, Bartholomeu DC, Gazzinelli RT, et al. Toll-like receptor 9-dependent immune activation by unmethylated CpG motifs in Aspergillus fumigatus DNA. Infect Immun 2008;76:2123–9. [PubMed: 18332208]
6. Nakamura K, Miyazato A, Xiao G, Hatta M, Inden K, Aoyagi T, et al. Deoxynucleic acids from Cryptococcus neoformans activate myeloid dendritic cells via a TLR9-dependent pathway. J Immunol 2008;180:4067–74. [PubMed: 18322216]

NIH-PA Author Manuscript

NIH-PA Author Manuscript

NIH-PA Author Manuscript

7. Krug A, Luker GD, Barchet W, Leib DA, Akira S, Colonna M. Herpes simplex virus type 1 activates murine natural interferon-producing cells through toll-like receptor 9. Blood 2004;103:1433–7. [PubMed: 14563635]
8. Lund J, Sato A, Akira S, Medzhitov R, Iwasaki A. Toll-like receptor 9-mediated recognition of herpes simplex virus-2 by plasmacytoid dendritic cells. J Exp Med 2003;198:513–20. [PubMed: 12900525]
9. Krug A, French AR, Barchet W, Fischer JAA, Dzionek A, Pingel JT, et al. TLR9–dependent recognition of MCMV by IPC and DC generates coordinated cytokine responses that activate antiviral NK cell function. Immunity 2004;21:107–19. [PubMed: 15345224]
10. Leadbetter EA, Rifkin IR, Hohlbaum AM, Beaudette BC, Shlomchik MJ, Marshak-Rothstein A. Chromatin-IgG complexes activate B cells by dual engagement of IgM and toll-like receptors. Nature 2002;416:603–7. [PubMed: 11948342]
11. Boule MW, Broughton C, Mackay F, Akira S, Marshak-Rothstein A, Rifkin IR. Toll-like receptor 9-dependent and -independent dendritic cell activation by chromatin-immunoglobulin G complexes. J Exp Med 2004;199:1631–40. [PubMed: 15197227]
12. Haas T, Metzger J, Schmitz F, Heit A, Muller T, Latz E, et al. The DNA sugar backbone 2 ′ deoxyribose determines toll-like receptor 9 activation. Immunity 2008;28:315–23. [PubMed: 18342006]
13. Rhee EG, Mendez S, Shah JA, Wu CY, Kirman JR, Turon TN, et al. Vaccination with heat-killed leishmania antigen or recombinant leishmanial protein and CpG oligodeoxynucleotides induces long-term memory $CD4^+$ and $CD8^+$ T cell responses and protection against leishmania major infection. J Exp Med 2002;195:1565–73. [PubMed: 12070284]
14. Weeratna RD, Makinen SR, McCluskie MJ, Davis HL. TLR agonists as vaccine adjuvants: comparison of CpG ODN and Resiquimod (R-848). Vaccine 2005;23:5263–70. [PubMed: 16081189]
15. Stacey KJ, Blackwell JM. Immunostimulatory DNA as an adjuvant in vaccination against leishmania major. Infect Immun 1999;67:3719–26. [PubMed: 10417129]
16. Chu RS, Targoni OS, Krieg AM, Lehmann PV, Harding CV. CpG oligodeoxynucleotides act as adjuvants that switch on T helper 1 (Th1) immunity. J Exp Med 1997;186:1623–31. [PubMed: 9362523]
17. Shen H, Iwasaki A. A crucial role for plasmacytoid dendritic cells in antiviral protection by CpG ODN-based vaginal microbicide. J Clin Invest 2006;116:2237–43. [PubMed: 16878177]
18. Wang YC, Abel K, Lantz K, Krieg AM, McChesney MB, Miller CJ. The toll-like receptor 7 (TLR7) agonist, imiquimod, and the TLR9 agonist, CpG ODN, induce antiviral cytokines and chemokines but do not prevent vaginal transmission of simian immunodeficiency virus when applied intravaginally to rhesus macaques. J Virol 2005;79:14355–70. [PubMed: 16254370]
19. Pyles RB, Higgins D, Chalk C, Zalar A, Eiden J, Brown C, et al. Use of immunostimulatory sequence-containing oligonucleotides as topical therapy for genital herpes simplex virus type 2 infection. J Virol 2002;76:11387–96. [PubMed: 12388699]
20. Ashkar AA, Bauer S, Mitchell WJ, Vieira J, Rosenthal KL. Local delivery of CpG oligodeoxynucleotides induces rapid changes in the genital mucosa and inhibits replication, but not entry, of herpes simplex virus type 2. J Virol 2003;77:8948–56. [PubMed: 12885911]
21. Bourquin C, Anz D, Zwiorek K, Lanz AL, Fuchs S, Weigel S, et al. Targeting CpG oligonucleotides to the lymph node by nanoparticles elicits efficient antitumoral immunity. J Immunol 2008;181:2990–8. [PubMed: 18713969]
22. de Jong S, Chikh G, Sekirov L, Raney S, Semple S, Klimuk S, et al. Encapsulation in liposomal nanoparticles enhances the immunostimulatory, adjuvant and anti-tumor activity of subcutaneously administered CpG ODN. Cancer Immunol Immunother 2007;56:1251–64. [PubMed: 17242927]
23. Diwan M, Elamanchili P, Lane H, Gainer A, Samuel J. Biodegradable nanoparticle mediated antigen delivery to human cord blood derived dendritic cells for induction of primary T cell responses. J Drug Targeting 2004;11:495–507.

NIH-PA Author Manuscript

NIH-PA Author Manuscript

NIH-PA Author Manuscript

24. Kwon YJ, Standley SM, Goh SL, Frechet JMJ. Enhanced antigen presentation and immunostimulation of dendritic cells using acid-degradable cationic nanoparticles. J Controlled Release 2005;105:199–212.
25. Sokolova V, Knuschke T, Kovtun A, Buer J, Epple M, Westendorf AM. The use of calcium phosphate nanoparticles encapsulating toll-like receptor ligands and the antigen hemagglutinin to induce dendritic cell maturation and T cell activation. Biomaterials 2010;31:5627–33. [PubMed: 20417963]
26. Wilsonl KD, de Jong SD, Kazem M, Lall R, Hope MJ, Cullis PR, et al. The combination of stabilized plasmid lipid particles and lipid nanoparticle encapsulated CpG containing oligodeoxynucleotides as a systemic genetic vaccine. J Gene Med 2009;11:14–25. [PubMed: 19003796]
27. Saito Y, Higuchi Y, Kawakami S, Yamashita F, Hashida M. Immunostimulatory characteristics induced by linear polyethyleneimine-plasmid DNA complexes in cultured macrophages. Hum Gene Ther 2009;20:137–45. [PubMed: 18937551]
28. Tan YD, Li S, Pitt BR, Huang L. The inhibitory role of CpG immunostimulatory motifs in cationic lipid vector-mediated transgene expression in vivo. Hum Gene Ther 1999;10:2153–61. [PubMed: 10498247]
29. Yasuda K, Ogawa Y, Yamane I, Nishikawa M, Takakura Y. Macrophage activation by a DNA/cationic liposome complex requires endosomal acidification and TLR9-dependent and -independent pathways. J Leukocyte Biol 2005;77:71–9. [PubMed: 15496451]
30. Zhang JS, Liu F, Conwell CC, Tan Y, Huang L. Mechanistic studies of sequential injection of cationic liposome and plasmid DNA. Mol Ther 2006;13:429–37. [PubMed: 16242997]
31. Walker WE, Booth CJ, Goldstein DR. TLR9 and IRF3 cooperate to induce a systemic inflammatory response in mice injected with liposome:DNA. Mol Ther 2010;18:775–84. [PubMed: 20145605]
32. Lahdeoja T, Pajarinen J, Kouri VP, Sillat T, Salo J, Konttinen YT. Toll-like receptors and aseptic loosening of hip endoprosthesis-a potential to respond against danger signals? J Orth Res 2010;28:184–90.
33. Tamaki Y, Takakubo Y, Goto K, Hirayama T, Sasaki K, Konttinen YT, et al. Increased expression of toll-like receptors in aseptic loose periprosthetic tissues and septic synovial membranes around total hip implants. J Rheumatol 2009;36:598–608. [PubMed: 19208601]
34. Pajarinen J, Mackiewicz Z, Pollanen R, Takagi M, Epstein NJ, Ma T, et al. Titanium particles modulate expression of toll-like receptor proteins. J Biomed Mater Res A 2010;92A:1528–37. [PubMed: 19425045]
35. Latz E, Schoenemeyer A, Visintin A, Fitzgerald KA, Monks BG, Knetter CF, et al. TLR9 signals after translocating from the ER to CpG DNA in the lysosome. Nat Immunol 2004;5:190–8. [PubMed: 14716310]
36. Heinrich PC, Castell JV, Andus T. Interleukin-6 and the acute phase response. Biochem J 1990;265:621–36. [PubMed: 1689567]
37. Vansnick J. Interleukin-6: an overview. Annu Rev Immunol 1990;8:253–78. [PubMed: 2188664]
38. Stetson DB, Medzhitov R. Type I interferons in host defense. Immunity 2006;25:373–81. [PubMed: 16979569]
39. Jilka RL, Hangoc G, Girasole G, Passeri G, Williams DC, Abrams JS, et al. Increased osteoclast development after estrogen loss - mediation by interleukin-6. Science 1992;257:88–91. [PubMed: 1621100]
40. Coelho LFL, Almeida GMD, Mennechet FJD, Blangy A, Uze G. Interferon-alpha and -beta differentially regulate osteoclastogenesis: role of differential induction of chemokine CXCL11 expression. Proc Natl Acad Sci USA 2005;102:11917–22. [PubMed: 16081539]
41. De Jong WH, Hagens WI, Krystek P, Burger MC, Sips A, Geertsma RE. Particle size-dependent organ distribution of gold nanoparticles after intravenous administration. Biomaterials 2008;29:1912–9. [PubMed: 18242692]
42. Tabata Y, Inoue Y, Ikada Y. Size effect on systemic and mucosal immune responses induced by oral administration of biodegradable microspheres. Vaccine 1996;14:1677–85. [PubMed: 9032899]

NIH-PA Author Manuscript

NIH-PA Author Manuscript

NIH-PA Author Manuscript

43. Tabata Y, Ikada Y. Effect of the size and surface charge of polymer microspheres on their phagocytosis by macrophage. Biomaterials 1988;9:356–62. [PubMed: 3214660]
44. Chono S, Tanino T, Seki T, Morimoto K. Influence of particle size on drug delivery to rat alveolar macrophages following pulmonary administration of ciprofloxacin incorporated into liposomes. J Drug Targeting 2006;14:557–66.
45. Champion JA, Walker A, Mitragotri S. Role of particle size in phagocytosis of polymeric microspheres. Pharm Res 2008;25:1815–21. [PubMed: 18373181]
46. Tran KK, Shen H. The role of phagosomal pH on the size-dependent efficiency of cross-presentation by dendritic cells. Biomaterials 2009;30:1356–62. [PubMed: 19091401]
47. Brewer JM, Pollock KGJ, Tetley L, Russell DG. Vesicle size influences the trafficking, processing, and presentation of antigens in lipid vesicles. J Immunol 2004;173:6143–50. [PubMed: 15528351]
48. Rejman J, Oberle V, Zuhorn IS, Hoekstra D. Size-dependent internalization of particles via the pathways of clathrin-and caveolae-mediated endocytosis. Biochem J 2004;377:159–69. [PubMed: 14505488]
49. Okuya K, Tamura Y, Saito K, Kutomi G, Torigoe T, Hirata K, et al. Spatiotemporal regulation of heat shock protein 90-chaperoned self-DNA and CpG-oligodeoxynucleotide for type I IFN induction via targeting to static early endosome. J Immunol 2010;184:7092–9. [PubMed: 20483722]
50. Honda K, Ohba Y, Yanai H, Negishi H, Mizutani T, Takaoka A, et al. Spatiotemporal regulation of MyD88-IRF-7 signalling for robust type-I interferon induction. Nature 2005;434:1035–40. [PubMed: 15815647]
51. Sasai M, Linehan MM, Iwasaki A. Bifurcation of toll-like receptor 9 signaling by adaptor protein 3. Science 2010;329:1530–4. [PubMed: 20847273]
52. Ohkuma S, Poole B. Fluorescence probe measurement of intralysosomal pH in living cells and perturbation of pH by various agents. Proc Natl Acad Sci USA 1978;75:3327–31. [PubMed: 28524]
53. Dalod M, Salazar-Mather TP, Malmgaard L, Lewis C, Asselin-Paturel C, Briere F, et al. Interferon alpha/beta and interleukin 12 responses to viral infections: pathways regulating dendritic cell cytokine expression in vivo. J Exp Med 2002;195:517–28. [PubMed: 11854364]
54. Trubetskoy VS, Loomis A, Hagstrom JE, Budker VG, Wolff JA. Layer-by-layer deposition of oppositely charged polyelectrolytes on the surface of condensed DNA particles. Nucleic Acids Res 1999;27:3090–5. [PubMed: 10454604]
55. Munier S, Messai I, Delair T, Verrier B, Ataman-Onal Y. Cationic PLA nanoparticles for DNA delivery: comparison of three surface polycations for DNA binding, protection and transfection properties. Colloids Surf B 2005;43:163–73.
56. Akinc A, Langer R. Measuring the pH environment of DNA delivered using nonviral vectors: implications for lysosomal trafficking. Biotechnol Bioeng 2002;78:503–8. [PubMed: 12115119]
57. Rouzina I, Bloomfield VA. DNA bending by small, mobile multivalent cations. Biophys J 1998;74:3152–64. [PubMed: 9635768]
58. Lipford GB, Sparwasser T, Bauer M, Zimmermann S, Koch ES, Heeg K, et al. Immunostimulatory DNA: sequence-dependent production of potentially harmful or useful cytokines. Eur J Immunol 1997;27:3420–6. [PubMed: 9464831]
59. Krug A, Rothenfusser S, Hornung V, Jahrsdorfer B, Blackwell S, Ballas ZK, et al. Identification of CpG oligonucleotide sequences with high induction of IFN-alpha/beta in plasmacytoid dendritic cells. Eur J Immunol 2001;31:2154–63. [PubMed: 11449369]
60. Ahmad-Nejad P, Hacker H, Rutz M, Bauer S, Vabulas RM, Wagner H. Bacterial CpG-DNA and lipopolysaccharides activate toll-like receptors at distinct cellular compartments. Eur J Immunol 2002;32:1958–68. [PubMed: 12115616]
61. Manzel L, Strekowski L, Ismail FMD, Smith JC, Macfarlane DE. Antagonism of immunostimulatory CpG-oligodeoxynucleotides by 4-aminoquinolines and other weak bases: mechanistic studies. J Pharmacol Exp Ther 1999;291:1337–47. [PubMed: 10565859]
62. Poole B, Ohkuma S. Effect of weak bases on the intralysosomal pH in mouse peritoneal macrophages. J Cell Biol 1981;90:665–9. [PubMed: 6169733]

NIH-PA Author Manuscript

NIH-PA Author Manuscript

NIH-PA Author Manuscript

63. Lakadamyali M, Rust MJ, Zhuang XW. Ligands for clathrin-mediated endocytosis are differentially sorted into distinct populations of early endosomes. Cell 2006;124:997–1009. [PubMed: 16530046]

64. Ahmad A, Evans HM, Ewert K, George CX, Samuel CE, Safinya CR. New multivalent cationic lipids reveal bell curve for transfection efficiency versus membrane charge density: lipid-DNA complexes for gene delivery. J Gene Med 2005;7:739–48. [PubMed: 15685706]

65. Lin AJ, Slack NL, Ahmad A, George CX, Samuel CE, Safinya CR. Three-dimensional imaging of lipid gene-carriers: membrane charge density controls universal transfection behavior in lamellar cationic liposome-DNA complexes. Biophys J 2003;84:3307–16. [PubMed: 12719260]

66. Zelphati O, Szoka FC. Mechanism of oligonucleotide release from cationic liposomes. Proc Natl Acad Sci USA 1996;93:11493–8. [PubMed: 8876163]

67. Kutomi G, Tamura Y, Okuya K, Yamamoto T, Hirohashi Y, Kamiguchi K, et al. Targeting to static endosome is required for efficient cross-presentation of endoplasmic reticulum-resident oxygen-regulated protein 150-peptide complexes. J Immunol 2009;183:5861–9. [PubMed: 19812200]

68. Fujihara SM, Nadler SG. Intranuclear targeted delivery of functional NF-kappa B by 70 kDa heat shock protein. EMBO J 1999;18:411–9. [PubMed: 9889197]

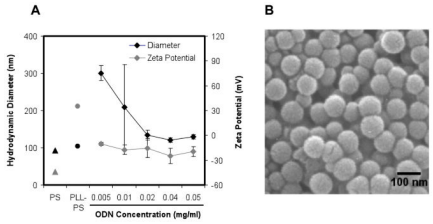

Figure 1.
Characterization of ODN-PLL-PS. (A) Characterization of the size and zeta potential of 100 nm 1826-PLL-PS. (B) A SEM image of 100 nm CpG-PLL-PS.

NIH-PA Author Manuscript
NIH-PA Author Manuscript
NIH-PA Author Manuscript

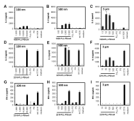

Figure 2.

The effect of particle size on the production of IL-6 and IFN-α. BC-1 cells were stimulated by 100 nm, 500 nm, and 3 μm (A–C) 1826- and (D–I) 2216-PLL-PS. PLL-PS and PS served as negative controls and were used at the highest particle-to-cell ratio of the corresponding particle size. Soluble ODNs (sol 1826 or sol 2216) at 0.005 mg/ml served as a positive control. The supernatants of cells were collected after 24 h and analyzed by ELISA for the (A–F) IL-6 and (G–I) IFN-α concentrations. The symbol * indicates thae no cytokine secretions were detected.

NIH-PA Author Manuscript
NIH-PA Author Manuscript
NIH-PA Author Manuscript

NIH-PA Author Manuscript

NIH-PA Author Manuscript

NIH-PA Author Manuscript

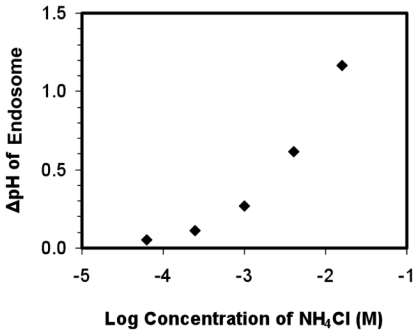

Figure 3.

The change in the pH of endosomes by the addition of NH_4Cl. Concentrations of NH4Cl (0.063, 0.25, 1, 4, 16 mM) are presented as Log_{10} of molar concentrations. The change in endosomal pH was calculated relative to the unmodified endosomal pH, which was 5.21.

NIH-PA Author Manuscript

NIH-PA Author Manuscript

NIH-PA Author Manuscript

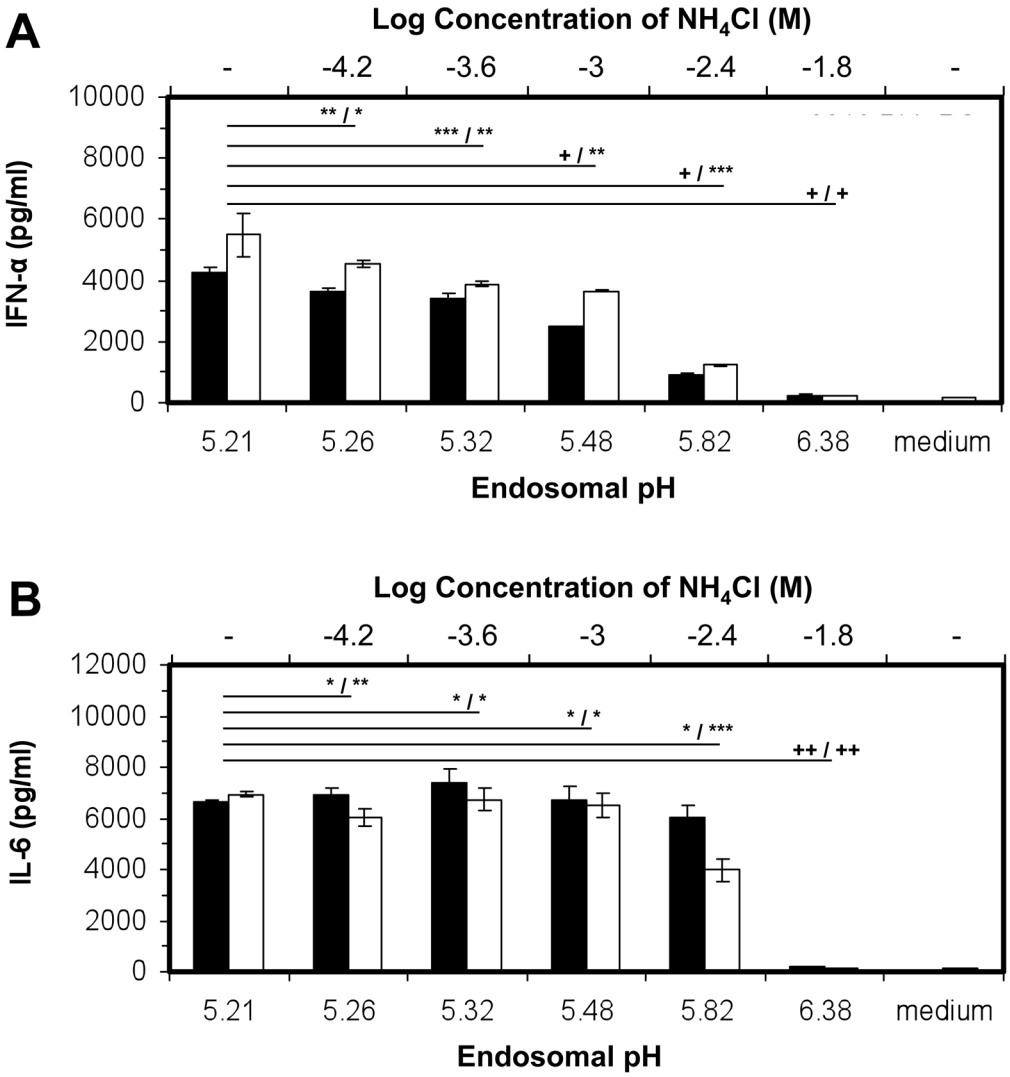

Figure 4.

The effect of endosomal pH on the production of cytokines. (■) 100 nm 2216- PLL-PS at 100,000 particles per cell, and (□) soluble ODN 2216 at 0.005 mg/ml, were added to BC-1 cells in the presence or absence of NH_4Cl. The cell supernatants were collected after 24 h and analyzed by ELISA for the (A) IL-6 and (B) IFN-α concentrations. The top and bottom x axes represent the Log10 of the molar concentration of NH_4Cl and the corresponding endosomal pH values, respectively. The symbols *, **, ***, +, and ++ indicate the level of the statistical significance of cytokine production concentrations: $1.0 > p > 0.1$, $0.1 > p > 0.05$, $0.05 > p > 0.01$, $0.01 > p > 0.001$, and $p < 0.001$, respectively. The statistical calculations were performed by using a two-tailed, unpaired Student's *t* test. All *p* values are shown relative to the unmodified pH of endosomes, and are presented as: *p* value for ODN-PLL-PS / *p* value for soluble ODNs.